

## The region ion sensitive field effect transistor, a novel bioelectronic nanosensor

K. Risveden<sup>a</sup>, J.F. Pontén<sup>a</sup>, N. Calander<sup>b</sup>, M. Willander<sup>b</sup>, B. Danielsson<sup>a,\*</sup>

<sup>a</sup> Department of Pure and Applied Biochemistry, Lund University, Center for Chemistry and Chemical Engineering,  
P.O. Box 124, SE-22100 Lund, Sweden

<sup>b</sup> Laboratory of Physical Electronics and Photonics, Department of Physics and Engineering Physics,  
Chalmers University of Technology and Göteborg University, SE-41296 Göteborg, Sweden

Received 29 May 2006; received in revised form 22 December 2006; accepted 23 January 2007

Available online 20 February 2007

### Abstract

A novel type of bioelectronic region ion sensitive field effect transistor (RISFET) nanosensor was constructed and demonstrated on two different sensor chips that could measure glucose with good linearity in the range of 0–0.6 mM and 0–0.3 mM with a limit of detection of 0.1 and 0.04 mM, respectively. The sensor is based on the principle of focusing charged reaction products with an electrical field in a region between the sensing electrodes. For glucose measurements, negatively charged gluconate ions were gathered between the sensing electrodes. The signal current response was measured using a low-noise pico ammeter (pA). Two different sizes of the RISFET sensor chips were constructed using conventional electron beam lithography. The measurements are done in partial volumes mainly restricted by the working distance between the sensing electrodes (790 and 2500 nm, respectively) and the influence of electrical fields that are concentrating the ions. The sensitivity was 28 pA/mM (2500 nm) and 830 pA/mM (790 nm), respectively. That is an increase in field strength by five times between the sensing electrodes increased the sensitivity by 30 times. The volumes expressed in this way are in low or sub femtoliter range. Preliminary studies revealed that with suitable modification and control of parameters such as the electric control signals and the chip electrode dimensions this sensor could also be used as a nanobiosensor by applying single enzyme molecule trapping. Hypotheses are given for impedance factors of the RISFET conducting channel.

© 2007 Elsevier B.V. All rights reserved.

**Keywords:** Nanosensor; Nanostructures; Electron beam lithography; Atomic force microscopy

### 1. Introduction

A biosensor is a compact analytical device incorporating a biological or biologically derived sensing element either integrated within or intimately associated with a physicochemical transducer. The usual aim of a biosensor is to produce either discrete or continuous digital electronic signals that are proportional to a single analyte or a related group of analytes as defined by Newman and coworkers (Newman et al., 2001). Typical analytes include saccharides, alcohols, amino acids, nucleotides (Jerome, 1996) glucose, L-lactate, cholesterol (Ricci and Palleschi, 2005) and neurotransmitters (Liu et al., 2005).

The interest in mini and micro format devices has increased in several areas of contemporary science and technology during the later years. While miniaturization could be described as scaling down of macro devices, microfabrication involves an entirely new set of concepts to achieve the desired goals (Xie et al., 2000). Xie and Danielsson (1996) demonstrated that micromachining and semiconductor technology can be merged for fabrication of integrated multianalyte thermal biosensors for simultaneous detection of glucose, urea and penicillin. A variety of mini and micro sensors has been proposed such as plastic chip sensors, microcolumn sensors, thermopile-based microbiosensors and thermistor-based microbiosensors (Xie et al., 2000).

The introduction of microbiosensors decreased the time of analysis, the size of the device and wastage of the reagent (Karube and Yokoyama, 1993). During the 1980s and 1990s much research was spent on the development of microbiosen-

\* Corresponding author. Tel.: +46 46 22 28 257; fax: +46 46 22 28 266.  
E-mail address: [Bengt.Danielsson@tbiokem.lth.se](mailto:Bengt.Danielsson@tbiokem.lth.se) (B. Danielsson).

sors such as field effect transistor (FET) sensors (Karube, 1991; Gotoh et al., 1999), amperometric microbiosensors, potentiometric microbiosensors (Karube et al., 1990; Reddy et al., 2005) and ion sensitive field effect transistor (ISFET) microbiosensors (Saito et al., 1991).

Nanobiosensors are an interesting area within the development of biosensors and is a progress from microbiosensors (de Souza, 2000; Vo-Dinh, 2002; Soundarrajan et al., 2005). Nanobiosensors have the potential for low cost mass production of lab-on-chip systems and integrating sensor array systems for handling small sample volumes, for instance single cell or single protein characterization or blood substrate analyses through the skin by reverse iontophoresis (Tierney et al., 2001).

Several authors have described the construction and uses of nanoscale structures with interesting sensing and reversible trapping properties (Chiragwandi et al., 2002; Hölzel et al., 2005; Rouhanizadeh et al., 2006). For example, a nanoscale water-based depletion-mode FET that uses the local changes in  $[H^+]$  as the gate for the detection of pH changes (Chiragwandi et al., 2002) and another structure using dielectrophoresis to trap a single protein molecule such as R-phycoerythrin have been described previously (Hölzel et al., 2005). Modification and application of such devices for reversible trapping a single enzyme molecule is an interesting direction for future nanobiosensors as no chip derivatization is required. The present work describes region ISFET (RISFET) sensors that are variants of the above mentioned nanostructures. The RISFET sensors functions as enhancement mode FETs. In RISFET sensors the ionic reaction products are selectively focused between the sensing electrodes using a region focusing electric field. An advantage of the RISFET sensor system to conventional amperometric detection methods is that it has an internal voltage reference of the sensor electrodes and does not require a reference electrode (Bergveld, 2003). In addition it can measure very small sample volumes and has dielectrophoretic trapping possibilities of single enzymes.

## 2. Experimental

### 2.1. Material

Glucose oxidase (GOD) from *Aspergillus niger*, Type V-S (1100 U/ml) and  $\beta$ -D-(+)-glucose were purchased from Sigma Chemical Company, Stockholm, Sweden. Tris base was purchased from Calbiochem®, Stockholm, Sweden. Water was purified (18.2 M $\Omega$ ) by an Elgastat Maxima Apparatus (Elga Ltd., Bucks, England). A 1 mM Tris/HCl buffer solution was prepared for chip E (pH 6.78) and for chip L (pH 6.52) using purified water. Glucose oxidase (2 U/ml) in 1 mM Tris/HCl buffer was prepared prior to experiments and glucose solution was subsequently added to achieve the required substrate concentration. N<sub>2</sub> gas of chemical grade (99.9996%) was purchased from AGA, Malmö, Sweden. All other chemicals used were of analytical grade.

### 2.2. Bioelectronic sensor chip

Two different chip structures were constructed using a low n-doped silicon wafer (Fig. 1). A silicon dioxide layer (80 nm), was thermally grown on the wafer. Titanium (3 nm) was used as gluing metal for the gold (80 nm) structures. The distance between the sensing electrodes placed in the center of the four outer metal plates were 790 nm (chip E, Fig. 1c) and 2500 nm (chip L, Fig. 1b). The larger outer chip structures were produced using conventional UV lithography (Fig. 1a), whereas the inner sensing electrodes were produced using conventional electron beam lithography.

### 2.3. Instrumental procedures and methods

All measurements were performed at ambient temperature:  $21 \pm 0.5$  °C.

A digital signal generator (K8016 PC function generator from Velleman Components BV Gavere, Belgium) was used for gen-

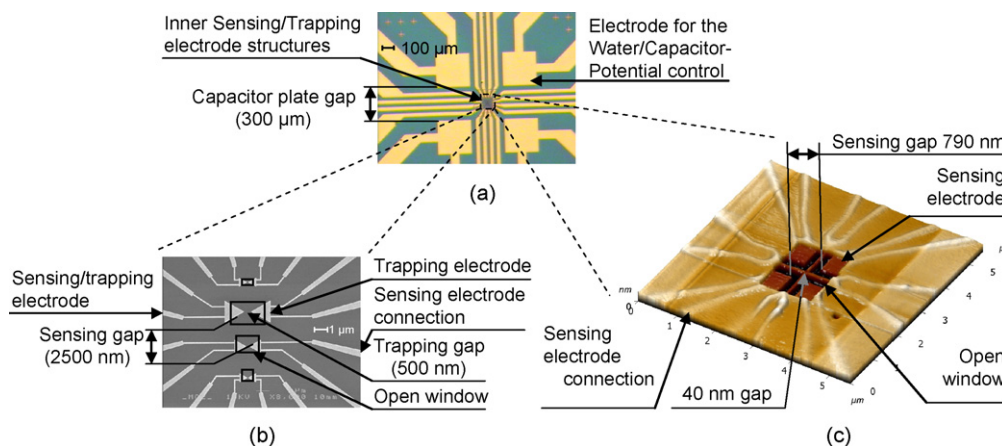


Fig. 1. (a) Optical microscope image showing the outer RISFET chip structure with the large water/capacitor potential control electrodes. (b) Scanning electron microscope image of the center structure (chip L) which was placed in the space at the centre of the outer RISFET structure. The sensing electrodes with an area of 1.3 and  $0.47 \mu\text{m}^2$ , respectively are placed at 2500 nm distance apart. The open window in the photoresist above the sensing electrodes is marked. (c) Atomic force microscopy image, showing a close-up of a variant of the RISFET center structure (chip E). In chip E the sensing electrodes with an area of  $0.36 \mu\text{m}^2$  are placed at 790 nm distance apart. In the center of chip E there is a cross structure made from four identical gold structures, that are separated by a 40 nm spacing.

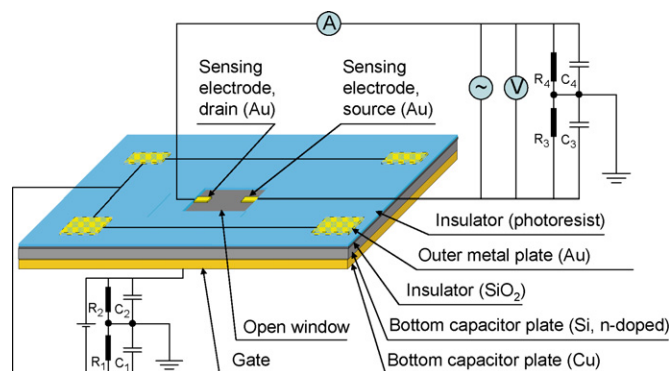


Fig. 2. The RISFET sensor setup of chip E. The apparatus used for determining the signal current response was an in house made pico ammeter in combination with a digital sampling scope. The sample droplet (20  $\mu$ l) is applied at the chip surface covering the sensing electrodes. Prior to sample acquisition, a voltage drop was applied between the bottom capacitor plate and the four outer metal plates causing a net positive charge on the bottom capacitor plate. A 0.1 Hz, 50 mV peak–peak ac voltage was set between the sensing electrodes. The sensing electrodes were in contact with the liquid whereas the four outer metal plates were insulated with photoresist.

erating the arbitrary waveforms to be used as signal voltage through the sensing electrodes (Fig. 1b and c).

An electrical field between the sample droplet and a bottom capacitor plate (Fig. 2.) was set from an external voltage generator (dc generator (PS3003—lab power supply, from HQ Power, Velleman Components NV)). The apparatus used for determining the signal current response was an in house made pico ammeter in combination with a digital sampling scope (PCS500 PC scope from Velleman Components BV) (Fig. 3).

#### 2.4. pA meter design

The pico ammeter (pA meter) used is based on a transimpedance amplifier IVC102 (Burr Brown, Tucson, US) and a common microcontroller Pic 16F84 (Microchip Technology Inc., Chandler, US). The transimpedance amplifier transforms incoming current to a proportional voltage according to the relationship:

$$V_0 = -I_{in} \frac{T_{int}}{C_{int}}$$

where  $I_{in}$  is the incoming current,  $C_{int}$  an internal capacitance (ca. 10 pF) and  $T_{int}$  is the integrating time. The output voltage from the pA meter is proportional to the incoming sensing current. In order to measure this considerably small current special care was taken on the instrumental setup. Two voltage dividers were composed from 3.3 k $\Omega$  metalized film resistors (RM0207S), and 100 nF metalized polyester capacitors (FKS 2, CECC approved) ( $R_1$ ,  $R_2$ ,  $R_3$ ,  $R_4$ ,  $C_1$ ,  $C_2$ ,  $C_3$  and  $C_4$  in Fig. 2).

#### 2.4.1. RISFET characterization

**2.4.1.1. Chip surface topography.** The RISFET chip surface topography was studied using an Atomic Force Microscope (AFM) with an NTEGRA-Configuration: NTEGRA-BIO-SNOM-EC in Resonant Mode (NTMDT, Russia) using

noncontact “Golden” silicon cantilevers (NSG 11) tips (ca. 5.5 N/m) (NTMDT).

**2.4.1.2. Sensing setup.** The RISFET setup is described in Fig. 2. The sample droplet (20  $\mu$ l) is applied at the chip surface above the sensing electrodes. A voltage is applied between the bottom capacitor plate and the four outer metal plates. The system consists of two capacitors in series oppositely charged. The first capacitor is made from the four outer metal plates, which is coupled in parallel, and the sample droplet with photoresist as insulator. The bottom capacitor plate (Si, n-doped) together with the sample droplet makes the other capacitor with SiO<sub>2</sub> as insulator.

**2.4.1.3. Gate electrical field.** The influence of the electric field applied between a sample droplet and the bottom capacitor plate was investigated by applying a 20  $\mu$ l water droplet on the surface of chip E (Fig. 1c). The electric field was generated by the gate dc-generator, which was set to the varying voltages between the sample droplet and the bottom capacitor plate. The voltage dividers and the ground (Fig. 2) define the potential of the bottom capacitor plate to be half the value of the potential applied by the gate dc-generator. dc signal voltage of  $-1.0$  V was applied between the sensing electrodes. When the dc signal current was stable, the dc voltage was swept from  $-1.0$  to  $+1.0$  V for 21 s and the dc signal current was measured as shown in Fig. 4.

#### 2.4.2. RISFET sensor response characteristics

The RISFET sensor function for glucose was studied for two different sensing electrode gaps, 790 and 2500 nm. Glucose (100 mM stock) was added incrementally to 10 ml buffer solution containing 2 U/ml glucose oxidase. After each addition, when the pH was stable 20  $\mu$ l sample liquid was applied on the chip surface. Prior to sample acquisition, the chip surface was charged. The sample droplet was given a  $-0.75$  V (the gate dc-generator =  $+1.5$  V) potential compared to the bottom capacitor plate (Fig. 2). A 0.1 Hz, 50 mV peak–peak ac voltage was applied between the sensing electrodes. The signal current, through the sample droplet, was observed. The sample droplet was removed and the chip surface was cleaned using vacuum, ultra pure H<sub>2</sub>O and N<sub>2</sub> (gas) prior to next sample acquisition. As control buffer solution without GOD was used.

### 3. Results and discussion

A novel type of bioelectronic RISFET nanosensor was constructed and demonstrated on two different sensor chips that could measure glucose with good linearity in the range of 0–0.6 mM and 0–0.3 mM with a limit of detection of 0.1 and 0.04 mM, respectively. The RISFET works as an enhancement mode FET.

#### 3.1. RISFET characterization

##### 3.1.1. Chip surface topography analysis

The chip surface topography of the center structures of chip E (Fig. 1c) and chip L (image not shown) were studied using an

AFM, similar investigations have previously been demonstrated (Bae et al., 2005). Care was taken not to bring the cantilever of the AFM into contact with the surface using semicontact mode. Thus, the surface topography of the photoresist was acquired without any distortion. Some measured distances are given in Section 2.3.

### 3.2. RISFET sensor function

#### 3.2.1. RISFET

When low sample concentrations are to be measured with very tiny electrode based chemical sensors, only a few ions will be in the effective sensing volume in between the sensing electrodes. Furthermore, when very low signal currents are used to minimize the signal electrical field strength the signal to noise ratio will become low. In order to increase the signal to noise ratio, without increasing the field strength between the sensing electrodes, the number of ions within the sensing volume can be increased through an other electric field arising from a charged bottom capacity plate. The electrical field gathers oppositely charged ions (counter ions) between the sensing electrodes, which increases the conductivity. The most important influence on the conductance is of cause depending on the chemical composition of the sample.

There are striking similarities between how a RISFET operates and an enhancement mode FET. The FET operates as a capacitor where one plate is a conducting channel between two ohmic contacts, the source and the drain electrodes (Fig. 3, Skoog et al., 1998; Horowitz, 1998; Meyburg et al., 2006).

The RISFET operates as a capacitor where one plate, the sample droplet, is a conducting channel between the sensing electrodes (source and drain) (Figs. 2 and 3). The density of the charge carriers (Fig. 5) in the conducting channel, and thus the conductivity, is modulated by the voltage applied to the bottom capacitor plate. The bottom capacitor plate and the sample liquid represent the gate. The gate is connected to the source via the two voltage dividers and the common ground. An increased voltage applied with the gate dc-generator results in an increased electrical field between the bottom capacitor plate and the sample droplet in the vicinity of the sensing electrodes. The electrical field attracts counterions and repels co-ions at the chip surface (Fig. 5). The net increase of charge carriers,

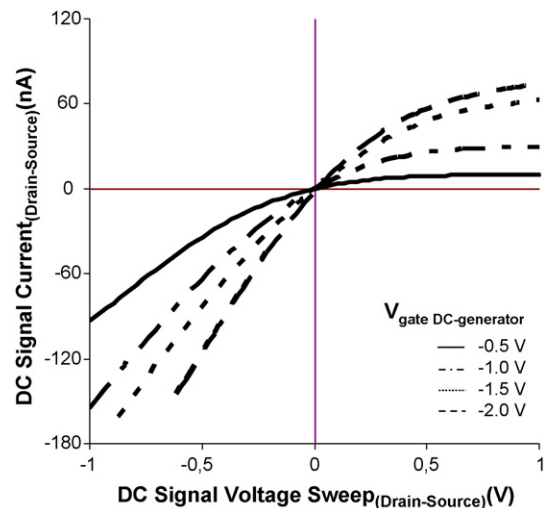


Fig. 4. The influence of the gate voltage influence on the signal current for deionized water during a ramped dc signal voltage. The influence of a negatively charged bottom capacitor plate on the signal current measured between the sensing electrodes (drain–source) in a region ion sensitive field effect transistor (RISFET) is demonstrated. A 790 nm sensing electrode gap was chosen using Chip E. 20  $\mu$ l water sample droplets were subsequently applied at the chip surface. Voltage (–0.5, –1.0, –1.5 and –2.0 V, respectively) was applied on the gate dc-generator. dc signal voltage of –1.0 V was applied between the sensing electrodes. When the dc signal current was stable, the dc voltage was swept from –1.0 to +1.0 V for 21 s. The slope of the curves shows a signal current dependency to the electrical charge of the bottom capacitor plate.

in the conducting channel along the chip surface, results in an enhanced drain–source signal current between the sensing electrodes (Fig. 4). Thus the sensitivity of the RISFET sensor is dependent on the charge of the bottom capacitor plate.

#### 3.2.2. Conducting channel

In deionized water counterions to the charge of the bottom capacitor plate forms the conducting channel. The signal current increase for the  $V_{\text{gate}}$  dc-generator (Fig. 4) is caused by the increased number of  $\text{H}^+$  in the conducting channel.

With increased voltage drop between the droplet and the bottom capacitor plate and with negative electric charge on the bottom capacitor plate compared to positive electrical charge on the sample droplet, the  $\text{H}^+$  ions gather close to the chip

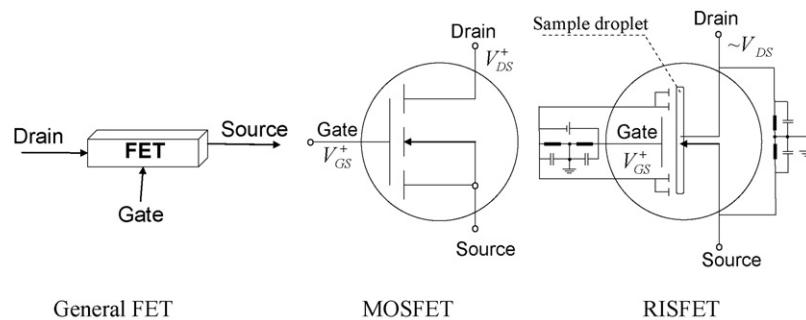


Fig. 3. Principle layout of a general FET and two different FET constructions: a  $n$ -channel enhancement mode metal oxide semiconductor field-effect transistor (MOSFET) and a RISFET. The RISFET is similar to a MOSFET, in that a gate voltage change results in a drain–source current change. However, the gate voltage is kept constant at chosen levels and the signal current instead of the threshold voltage is affected by the sample composition.

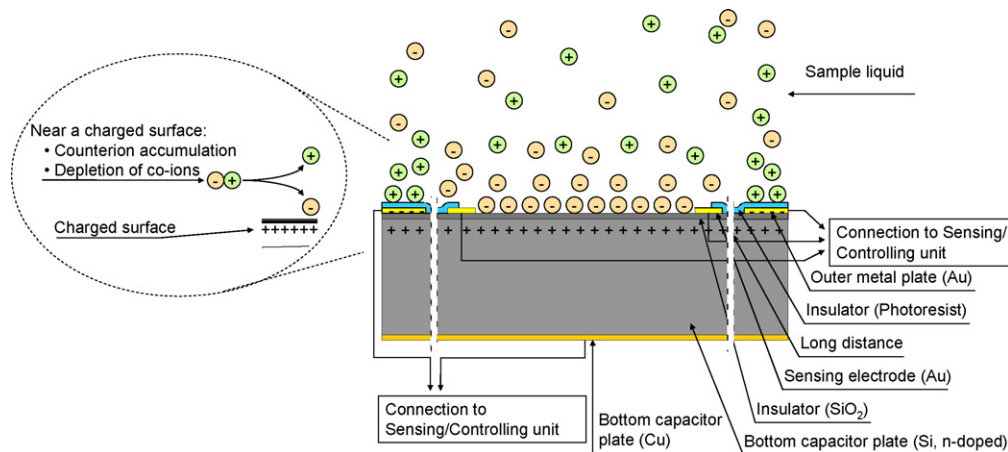


Fig. 5. Description of the RISFET sensor. At the chip surface between the sensing electrodes there is accumulation of counterions and depletion of co-ions resulting in a net increase of ions causing a conducting channel for the signal current.

surface with the corresponding increase in the signal current. For the same voltage drop but with opposite polarity between the droplet and the bottom capacitor plate, and the same voltage drop between the sensing electrodes the signal current was less (data not shown). The reason is probably due to the lower mobility of  $\text{OH}^-$  ions as compared to the  $\text{H}^+$  ions (Laidler and Meiser, 1995). For a sample volume sphere of diameter equal to the distance between the 790 nm RISFET sensing electrodes, the volume would be in the range of 0.3 fl. A 0.3 fl water droplet at pH 7 contains only 16  $\text{H}^+$  ions. The electrical field that arises from the charged bottom capacitor plate increases the conductivity and hence the signal current density in the region of the sample volume that is located in the vicinity of the sensing electrodes.

### 3.2.3. Ion concentration profile

The impedance between the sensing electrodes is influenced by the mobility of the ions in the sample liquid. By increasing the electrical field between the sample droplet and the bottom capacitor plate, the signal current response is enhanced as demonstrated in Fig. 4. This phenomenon can be explained by the increased number of charge carriers between the low profile (80 nm high) sensing electrodes. As the bottom capacitor plate is charged, ions of opposite charge (counterions) are focused to a region close to the chip surface (Fig. 5) and the signal to noise ratio is increased.

The ions at the chip surface are mainly an increased concentration of counterions to the charge of the bottom capacitor plate (e.g. gluconate<sup>-</sup>,  $\text{Cl}^-$  and  $\text{OH}^-$  at a positively charged bottom capacity plate). If the chip surface is negatively charged through dissociation of e.g.  $\text{H}^+$  ions then the amount of counterions are of a magnitude sufficient to balance most of the surface charge (Israelachivili, 1995). This dissociation affect has not been observed to influence the conductivity. By changing the polarity of the chip surface potential, positive or negative ions can be chosen as counterions. Therefore the demonstrated sensor is suitable for monitoring or estimating any reaction that proceeds through charged species, e.g. the formation of gluconate<sup>-</sup> from glucose as described in Section 3.2.4. The density of ions at any distance  $h$  from an insulated charged surface is explained

in detail by Israelachivili (1995). The density of ions at any distance  $h$  from a charged surface, is given by the expression:

$$\rho_{hi} = \rho_{\infty i} e^{-z_i e \Psi_h / kT}$$

where the ion valency is  $\pm z_i$ , the  $e$  in the exponent is the electron charge,  $\Psi_h$  the sample liquid potential at any distance  $h$  from the insulated surface,  $k$  the Boltzmann's constant, and  $T$  is the Kelvin temperature. The sample liquid potential  $\Psi_h$  can be calculated using the Gouy–Chapman theory for high potentials (Torrie and Valleau, 1979), while it reduces to the so-called Debye–Hückel equation for low potentials (below about 25 mV). The total ionic concentration at any distance  $h$  from the surface is given by  $\sum_i \rho_{hi}$  and is for the RISFET tentatively illustrated in Fig. 5.

### 3.2.4. Impedance of the conducting channel

The impedance of the conducting channel is determined by the mobility of the ions. The ionic composition in the sensing region and thus the specificity of the RISFET sensor is a function of the chip surface potential and the RISFET sensor design. In Section 3.2.2 it was reported that a negative voltage applied on the bottom capacity plate yields a higher signal current than a positive voltage for a deionized water system. The reason is the difference in mobility between the counterions for the two systems. In the first case,  $\text{H}^+$  functions as counterions and in the latter case  $\text{OH}^-$  ions. The higher mobility of the  $\text{H}^+$  ions, and the difference in the signal current, demonstrates the selectivity of the RISFET system for counterions. A similar experiment was carried out on an acetate and choline system, where gathering of the negative ions (acetate) yielded a higher conductivity than the positive ions (data not shown).

The electrical charge of the bottom capacitor plate causes attraction of counterions and repulsion of co-ions to the chip surface that in turn creates a conducting channel in between the sensing electrodes. The conductivity of this channel does not have a typical hyperbolic sine relation between the ionic current density and the electric field as might be expected (Bockris and Reddy, 1976). Instead of the inflection point in the origin, the curves in Fig. 4 (showing  $\text{H}^+$  as counterions and  $\text{OH}^-$  as co-ions)

are asymmetrically bended through the origin. The bending of the curves can be explained by the ramping of the DC signal from negative to positive voltage that causes a ramped electric field between the sensing electrodes. During the ramping the speed of the ions is continuously changed, which continuously changes the conducting channel. In Fig. 4 the bending of the curves show a decreased conductivity in the conducting channel along the ramping, indicating that the ions are disappearing from the conducting channel. The scattering of the ions might be enhanced by vortex rotation (Chiragwandi et al., 2005).

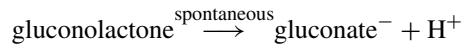
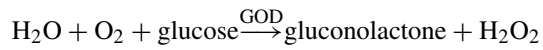
The counterions pulls the surrounding water molecules through frictional forces. A counterion with charge  $q$  (C) in an electric field  $E$  ( $\text{Vm}^{-1}$ ) feels an acceleration force  $qE$  (N). At constant electric field  $E$ , a steady-state speed is reached for the ions and the surrounding water, when the accelerating force ( $qE$ ) equals the frictional force generated by the separation medium (water), or  $qE = fu_E$  where  $f$  = the friction coefficient and  $u_E$  = the electrophoretic steady state speed of the counterion. The conducting channel reminds of a half profile electroosmotic flow (EOF) pump with ramped voltage between the anode and the cathode. EOF systems have thoroughly been described in literature (Mosher et al., 1992; Laidler and Meiser, 1995; Dittman and Rozing, 1996; Heiger, 2000; Madao, 2002).

### 3.2.5. Sample liquid composition

Different ionic solutions (sample droplets) yield different impedance properties to the system as a function of the difference in concentration and in the ion mobility in the sensing region. Ionic products of chemical reactions can therefore be correlated to the signal current response, e.g. the formation of gluconate<sup>-</sup> from glucose as described in Section 3.2.6.

The influence of the ionic composition on the signal current response was demonstrated on a glucose oxidase-glucose system, where glucose was converted to gluconolactone on the action of glucose oxidase in 1 mM Tris/HCl buffer. Gluconolactone was spontaneously converted to gluconate<sup>-</sup> and H<sup>+</sup> as

described in the following equations:



The production or consumption of ions through a chemical or biochemical reaction, in combination with a region focusing electrical field, defines the sensing principle of the RISFET. The RISFET gate partly distinguishes the negatively charged gluconate<sup>-</sup> (counterions) from the H<sup>+</sup> ions (co-ions) in the conducting channel as the bottom capacitor plate is positively charged. The increase of gluconate<sup>-</sup> ions in the sample liquid can be followed as an increase in the signal response current.

### 3.2.6. The glucose signal response characteristics of the RISFET sensor

The RISFET's amperometric response characteristic for different glucose concentrations were examined for two different 80 nm thick electrode structures; chip E (790 nm electrode gap, Fig. 1c) and chip L (2500 nm electrode gap, Fig. 1b). To reduce the effect of current electrolysis, vortex rotation and heating of the sample, the signal voltage was kept low. Furthermore we have found that the linearity is better under these low-field conditions. This phenomenon is described by Bockris and Reddy, 1976. The ac signal voltage was kept constant at 50 mV peak–peak ac (at steady state). Samples with different glucose concentrations were applied to the chip and the ac RMS signal current was obtained. When GOD was present, the sample glucose concentration was increased from 0–0.3 mM for chip E and 0–0.6 mM for chip L (Fig. 6), resulting in a corresponding linear increase in the signal current response from 210 to 440 pA and 7 to 24 pA, respectively.

As control, glucose was prepared at different concentrations, with no GOD present. In this case the signal current response remained constant at 200 pA for chip E, and 7 pA for chip

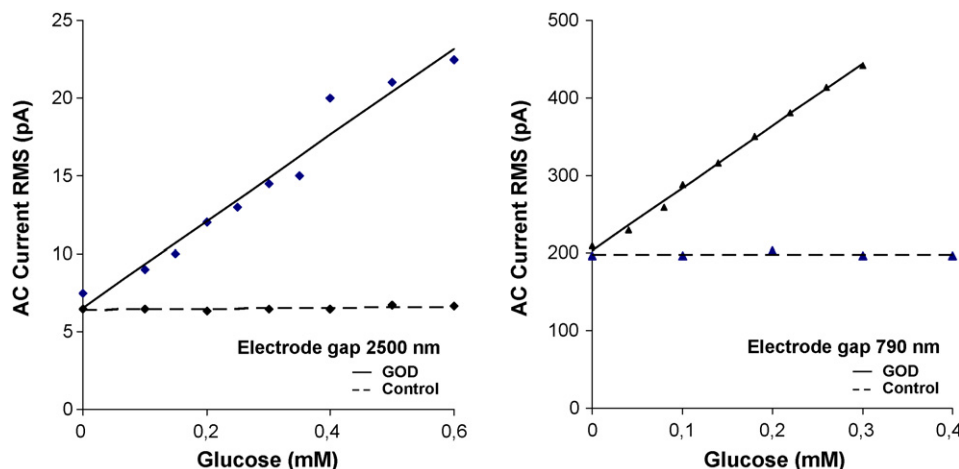


Fig. 6. The linear signal current response as a function of pH and glucose concentration for chip L (2500 nm) and chip E (790 nm). The response was measured for the 20  $\mu\text{l}$  of enzymatically (GOD) oxidized glucose samples and control samples without GOD applied at the RISFET sensor chip surface. To reduce the effect of current electrolysis and heating of the sample, the signal voltage was kept low. The ac signal voltage was kept constant at 50 mV peak–peak ac voltage, 0.1 Hz, (at steady state) and a potential of 1.5 V was applied between the bottom capacitor plate and the four outer metal plates (yielding a positively charged bottom capacitor plate).

L, respectively. Thus, there was a significant signal difference between the oxidized glucose solutions and the control. For the same applied voltage, chip E and chip L exhibited different signal current response characteristics owing to the difference in the field strength of the corresponding sensing electrode gap. Chip E (790 nm) with the smaller sensing electrode gaps and hence larger field strengths compared to chip L (2500 nm) showed better glucose sensitivity (Fig. 6). In Fig. 6 the field strength of the smaller sensing gap is five times higher than the field strength of the larger electrode gap, however the sensitivity is increased 30 times. A part of the explanation of this large increase in sensitivity is that the ion layer along the insulating plate between the electrodes has a raise. This is not the case with the improved chip E with the smaller distance between the sensing electrodes. On the top of the raise the ion layer must be thinned out due to a decreased electrical field from the bottom capacitor plate. One advantage of making small electrode gaps is that it is easier to make a small flat surface than a large flat surface, which in turn affects the homogeneity of the conducting ion layer. The risk with a large rough surface is that the ions are concentrated into sinks and that they avoid rises due to differences in the electrical field.

The field strength between the sensing electrodes is influenced by the electrode geometry, which can be balanced with the signal voltage. In order to avoid electrical influence on the sample, the product of the signal current and the applied voltage should be kept as low as possible, yielding low signal currents. These low currents require highly sensitive current sensing instruments. The pA measurement device used in this study (Section 2.4) satisfies this demand. The higher sensitivity of chip E compared to chip L (Fig. 6) can be explained by the higher field strengths between the sensing electrodes of chip E. The increased field strength reduces the signal to noise ratio of the system.

The chips L and E demonstrate the influence of the sensing electrodes geometry. A standard chip structure was used for many different devices; one of them is our RISFET sensor. All electrodes in the two chips were not used, such as the four 60 nm gold patches symmetrically placed, between the sensing electrodes, as a cross without connection in the center (Fig. 1c). In chip L (2500 nm), triangular electrodes were placed with the flat sides towards each other. In chip E (790 nm), the electrode distance was decreased to one third. Simultaneously the electrodes were shaped as squares and placed so that the edges were faced towards each other. In addition, the influence of the surface charge was enhanced for chip E, by completely removing all photoresist walls in between the sensing electrodes. As a result the field strength was increased about 5 times in chip E compared to chip L but the sensitivity was enhanced by 30 times. The sensitivity for chip L was 28 pA/mM and the sensitivity for chip E was 830 pA/mM glucose at 0.1 Hz, 50 mV peak–peak ac signal voltage between the sensing electrodes and the bottom capacitor plate was positively charged with 0.75 V.

These preliminary studies reveal that with suitable modification and control of parameters such as the electric control signals and the chip geometry this sensor could also be used as a nanobiosensor by applying single enzyme molecule trap-

ping. Chip L was previously demonstrated for single protein trapping using dielectrophoresis. The trapping was demonstrated on R-phycoerythrin, a fluorescent protein that is of the same size (Hecht et al., 1993; Chang et al., 1996) as glucose oxidase—indicating that the trapping force (0.1 pN) will be of the same order of magnitude also for glucose oxidase, which is well above the threshold force of the Brownian motion (0.3 fN) as described by Hölzel et al. (2005). Here it has been demonstrated that chip L also could be used for monitoring the conversion of glucose to gluconate through the use of glucose oxidase. It was also shown that changing the geometry of the sensing electrodes and the chip surface increased the sensitivity of the sensor several fold. The design of the electrical setup of this biosensor could be approached in several different ways depending on what electronic control parameters are available. One design would be to use two electrodes for capturing and two for sensing, however physically only three electrodes would be used, placed in a triangular position where one trapping electrode and one sensing electrode would be the same as indicated in Fig. 1b.

#### 4. Conclusions and future perspectives

Significant signal difference was obtained for glucose and oxidized glucose when choosing a triangular electrode setup which could also serve as a trapping device for the future single enzyme based sensors. Though it is very early to suggest, it might be possible to control the sensitivity of the RISFET structure by a suitable combination of applied voltage, electronic control, choice and design of sensing electrodes and the distance between them. The linear current response obtained for the glucose measurements is a good indication that the RISFET sensor system could be used also for other enzyme systems that involve charged species. A drawback of the present system is the choice of photoresist as insulator of the top layer, since it is soft and easily ruptured by a pipette tip. Changing the insulator for a SiO<sub>2</sub> or a SiN<sub>x</sub> layer, or introducing a closed flow cell system, would probably reduce this problem, since these materials are hard and not easily ruptured by a pipette tip. We are presently building up a flowcell system, which would deplete the need of using pipette tips. The RISFET sensor can at present state not measure neutral products.

The size of the sensor electrode gap gives an idea of the smallest possible sample volume, which could be applied to the RISFET sensor. The size of the sample droplet could be estimated as a sphere of a diameter equal to the distance between the RISFET sensing electrodes (a sphere with a diameter, equal to the distance between the electrodes (790 nm) has the volume 0.3 fl, which is in the size of a small bacteria, e.g. *Clostridium Botulinum* (Prescott et al., 1999)). The smallest possible droplet is in the order of 4 magnitudes smaller than the earlier reported miniaturized biosensors with the internal volumes in the range of 10–20 nl (Rhemrev-Boom et al., 2001). The capability of measuring fl sample volumes could be used for pH measurements and single enzyme based measurements at the surface of single spores, prokaryote or eukaryote cells. This can help us to understand how drugs act on a single cell level.

## Acknowledgements

The authors are grateful to the financial supports of the Swedish Research Council (Contracts No. 230-2000-340 and No. 621-2001-2753) and the European Commission (NANOCELL QLRT-2001-00278).

The authors wish to thank the undergraduate students K. Petersson and L. Eisele for excellent technical assistance. The authors also wish to thank Prof. S. Nilsson and Prof. P.-O. Larsson for helpful comments.

## References

- Bae, Y.M., Oh, B.-K., Lee, W., Lee, W.H., Choi, J.-W., 2005. *Biosens. Bioelectron.* 21 (1), 103–110.
- Bergveld, P., 2003. *Sens. Actuators B* 88, 1–20.
- Bockris, J.O'M., Reddy, A.K.N., 1976. *Modern Electrochemistry*, vol. 1, A Plenum/Rosetta ed., Second Paperback Printing. Plenum Publishing Corporation, London, pp. 287–512.
- Chang, W.-R., Jiang, T., Wan, Z.-L., Zhang, J.-P., Yang, Z.-X., Liang, D.-C., 1996. *J. Mol. Biol.* 262 (5), 721–731.
- Chiragwandi, Z.G., Nur, O., Willander, M., Calander, N., 2002. *Appl. Phys. Lett.* 83 (25), 5310–5312.
- Chiragwandi, Z.G., Nur, O., Willander, M., Panas, I., 2005. *Appl. Phys. Lett.* 87 (15), 153109-1–153109-3.
- de Souza, P.R., 2000. *FEBS Lett.* 475 (1), 43–46.
- Dittman, M.M., Rozing, G.P., 1996. *J. Chromatogr. A* 744, 63–74.
- Gotoh, M., Tamiya, E., Karube, I., 1999. *J. Membr. Sci.* 41, 291–303.
- Hecht, H.J., Kalisz, H.M., Hendle, J., Schmid, R.D., Schomburg, D., 1993. *J. Mol. Biol.* 229 (1), 153–172.
- Heiger, D., 2000. *High performance capillary electrophoresis—an introduction*. Publication No. 5968-9963E. Agilent Technologies, Colorado Springs, CO, USA.
- Hölzel, R., Calander, N., Chiragwandi, Z., Willander, M., Bier, F., 2005. *Phys. Rev. Lett.* 95 (12), 128102/1–128102/4.
- Horowitz, G., 1998. *Adv. Mater.* 10 (5), 365–377.
- Israelachvili, J.N., 1995. *Intermolecular and Surface Forces*, 2nd ed. Academic Press, Harcourt Brace & Company, Publishers, London, pp. 231–238.
- Jerome, S.S., 1996. In: Taylor, F.T. (Ed.), *Handbook of Chemical and Biological Sensors*. Institute of Physics Publishing, Bristol and Philadelphia.
- Karube, I., 1991. *Polym. J.* 23 (5), 573–581.
- Karube, I., Yokoyama, K., 1993. *Sens. Actuators B: Chem.* 13 (1–3), 12–15.
- Karube, I., Sode, K., Tamiya, E., 1990. *J. Biotechnol.* 15 (3), 267–281.
- Laidler, K., Meiser, J.H., 1995. *Physical Chemistry*, 2nd ed. Houghton Mifflin Company, Boston, pp. 284–301, 854–855, 897–900.
- Liu, A., Honma, I., Zhou, H., 2005. *Biosens. Bioelectron.* 21 (5), 809–816.
- Madao, M.J., 2002. *Fundamentals of Microfabrication: the Science of Miniaturization*, vol. 501., 2nd ed. CRC Press LLC, Boca Raton, pp. 562–565.
- Meyburg, S., Goryll, M., Moers, J., Ingebrandt, S., Bocker-Meffert, S., Luth, H., Offenhausser, A., 2006. *Biosens. Bioelectron.* 21 (7), 1037–1044.
- Mosher, R.A., Saville, D.A., Thurman, W., Radola, B.J., 1992. *The Dynamics of Electrophoresis*. Radola, B.J., VCH Verlagsgesellschaft mbH, Weinheim.
- Newman, J.D., Tigwell, L.J., Warner, P.J., Turner, A.P.F., 2001. *Sens. Rev.* 21 (4), 268–271.
- Prescott, L., Harley, J., Klein, D., 1999. *Microbiology*, 4th ed. Kane T. Kevin. WCB/McGraw-Hill, A division of the McGraw-Hill Companies Inc., Columbus.
- Reddy, K.R.C., Turcu, F., Schulte, A., Kayastha, A.M., Schuhmann, W., 2005. *Anal. Chem.* 77, 5063–5067.
- Rhemrev-Boom, M.M., Korf, J., Venema, K., Urban, G., Vadgama, P., 2001. *Biosens. Bioelectron.* 16 (9–12), 839–847.
- Ricci, F., Palleschi, G., 2005. *Biosens. Bioelectron.* 21 (3), 389–407.
- Rouhanizadeh, M., Tang, T., Li, C., Hwang, J., Zhou, C., Hsiai, T.K., 2006. *Sens. Actuators B: Chem.* B114 (2), 788–798.
- Saito, A., Miyamoto, S., Kimura, J., Kuriyama, T., 1991. *Sens. Actuators B: Chem.* B5 (1–4), 237–239.
- Skoog, D.A., Holler, F.J., Nieman, T.A., 1998. *Principles of Instrumental Analysis*, 5th ed. McDonald A., Harcourt Brace & Company, Orlando.
- Soundarrajan, P., Ginsberg, V., Yaniv, Z., 2005. *PCT Int. Appl.*, pp. 34.
- Tierney, M.J., Tamada, J.A., Potts, R.O., Jovanovic, L., Garg, S., Cygnus Research Team, 2001. *Biosensors and Bioelectronics* 16 (9–12), 621–629.
- Torrie, G.M., Valleau, J.P., 1979. *Chem. Phys. Lett.* 65 (2), 343–346.
- Vo-Dinh, T., 2002. *J. Cell. Biochem. (Suppl. 39)*, 154–161.
- Xie, B., Danielsson, B., 1996. *Anal. Lett.* 29 (11), 1921–1932.
- Xie, B., Ramanathan, K., Danielsson, B., 2000. *TrAC* 19 (5), 340–349.